Transition-Selective Pulses in Zero-Field Nuclear Magnetic Resonance

Journal:	*The Journal of Physical Chemistry*
Manuscript ID	jp-2016-040177.R1
Manuscript Type:	Article
Date Submitted by the Author:	25-May-2016
Complete List of Authors:	Sjolander, Tobias; University of California at Berkeley, Chemistry Tayler, Michael; University of California Berkeley, King, Jonathan; University of California at Berkeley, Chemistry; Materials Science Division, Lawrence Berkeley National Laboratory Budker, Dmitry; Univeristy of California, Berkeley, Physics; Helmholtz Institute Mainz, University of Mainz Pines, Alexander; University of California at Berkeley, Chemistry

Transition-Selective Pulses in Zero-Field Nuclear Magnetic Resonance

Tobias F. Sjolander, [*,†] Michael C. D. Tayler, [‡,¶] Jonathan P. King, [†,§] Dmitry Budker, [*,‡,∥,§] and Alexander Pines [†,§]

†*Department of Chemistry, University of California at Berkeley, Berkeley, California 94720-3220, United States*

‡*Department of Physics, University of California at Berkeley, Berkeley, California 94720-7300, United States*

¶*Magnetic Resonance Research Centre, Department of Chemical Engineering and Biotechnology, University of Cambridge, Pembroke Street, Cambridge CB2 3RA, UK*

§*Materials Science Division, Lawrence Berkeley National Laboratory, Berkeley California 94720-3220*

∥*Helmholtz Institute Mainz, Johannes Gutenberg University, 55099 Mainz, Germany*

Abstract

We use low-amplitude, ultra-low frequency pulses to drive nuclear spin transitions in zero and ultra-low magnetic fields. In analogy to high-field NMR, a range of sophisticated experiments becomes available as these allow narrow-band excitation. As a first demonstration, pulses with excitation bandwidths 0.5-5 Hz are used for population redistribution, selective excitation, and coherence filtration. These methods are helpful when interpreting zero - and ultra-low-field NMR spectra that contain a large number of transitions.

Introduction

Nuclear magnetic resonance (NMR) techniques provide an abundance of information on the chemical and structural composition of matter. High-field chemical shifts probe the electronic environment, the magnitudes of spin-spin coupling constants correlate strongly with both bond distances and bond angles, and geometric constraints are given by rates of inter-nuclear cross-relaxation.[1–3] A strength of NMR is the ability to selectively measure the data of interest by choosing out of hundreds of experimental protocols.[4] Many of these protocols require exciting only a select portion of the frequency spectrum, using narrow-band pulses. Frequency selectivity is implicitly assumed in the design of high-field NMR pulse sequences, as the resonance frequencies of different spin species are widely separated. Many techniques also rely on selectivity beyond differentiating spin species, to the extent of addressing individual transitions.[4–7] Selective irradiation is the basis for many polarization-transfer methods (e.g. INAPT, Insensitive Nuclei Assigned by Polarization Transfer[8,9]), spin-spin correlation experiments (e.g. SELCOSY[10]) and solvent suppression techniques.

Narrow-band pulses have yet to be explored in zero to ultra-low field (ZULF) NMR where the leading fields are $< 1\mu$T. The ZULF regime is characterized by spin-spin couplings dominating over the Zeeman interaction between spins and the external magnetic field,[11–14] contrary to traditional high-field NMR where the Zeeman interaction is dominant. Advantages of ZULF NMR include longer coherence times leading to mHz spectral resolution and the

ability to measure nonsecular spin interactions that are otherwise masked by high magnetic fields.[15,16] Instrumentation for ZULF NMR detection includes magnetometers based on optically pumped alkali vapors[17–19] and superconducting quantum interference devices.[20–23] The use of an atomic magnetometer as a low-cost, cryogen-free NMR spectrometer is described in the literature.[13,24–27] Despite the absence of chemical shifts in ZULF, chemically resolved NMR spectra are obtained. For a molecule in the isotropic liquid phase in zero-field, the molecular fingerprint is a spectrum with characteristic frequencies given by the untruncated J-coupling Hamiltonian. J-couplings are typically in the frequency range of 0-1000 Hz and the linewidths achieved are routinely between 0.01 and 0.1 Hz, making ZULF NMR a high-resolution spectroscopic method for chemical analysis.[15,28,29] The ZULF technique extends to spectroscopy in the presence of small perturbing fields[30,31] and residual dipole-dipole interactions,[16] which can increase spectral information content.

In this paper we demonstrate frequency selective pulses in the ZULF regime with a typical excitation bandwidth 0.5-5 Hz, detecting the NMR signals with a sensitive ^{87}Rb atomic magnetometer. As an application we introduce an experiment that identifies groups of connected transitions between the ZULF energy levels of a spin system. This is conceptually similar to spin-tickling experiments performed in high-field NMR, where connected transitions are used to identify the spin topology and energy-level structure.[32,33] Simplification of ZULF NMR spectra into such groups assists with assignment and helps resolve ambiguity with interpretation, particularly in the case of molecules with large numbers of transitions. We demonstrate further selectivity by taking advantage of the selection rules for circularly polarized pulses[34] allowing us to address narrow splittings caused by small DC magnetic fields

Prior to this work, ZULF NMR experiments have used DC magnetic field pulses for excitation and manipulation of the spin system. Pulsed fields stronger than 100 μT are sufficient to rotate nuclear spins effectively instantaneously with respect to the time scale of free evolution, so that the result is a rotation about the field axis through angles $\theta_i = \gamma_i B t$ where γ_i is the gyromagnetic ratio of the i^{th} spin, B is the field strength, and t is the duration of the pulse. This method of manipulating spins has limitations. It is necessarily broadband with respect to the ZULF spectrum and the range of available operations depends on the ratios of the γ_is of the spins involved. For example, using DC pulses one can perform a simultaneous $\theta \approx 4\pi$ rotation on ^{1}H and $\theta = \pi$ on ^{13}C, however a $\theta \approx \pi$ rotation on both nuclei, as required by many decoupling and refocusing sequences, is more challenging; using a single DC pulse it is impossible to simultaneously rotate ^{1}H and ^{13}C spins through the same angle, other than near-$2\pi/3$ multiples (e.g. $\theta_{\text{H}} \approx 8\pi/3$, $\theta_{\text{C}} \approx 2\pi/3$; $\gamma_{\text{H}}/\gamma_{\text{C}} \approx 3.97$). Composite pulses have been suggested[35] but performing arbitrary rotations is not a solved problem and generally speaking the control of multiple spin species is significantly restricted.

Theory

The resonant pulses demonstrated in this work drive spin populations directly between the zero-field eigenstates and therefore allow greater control over which transitions are excited. We write the liquid state zero-field Hamiltonian, in angular frequency units, as

$$H_J = 2\pi \sum_{i,j>i} J_{ij} \boldsymbol{I}_i \cdot \boldsymbol{I}_j, \qquad (1)$$

where the $\boldsymbol{I}$ are the total angular momentum operators for groups of equivalent spins and the J are scalar spin-spin coupling constants. The eigenstates of H_J are total spin angular momentum states denoted $|F, m_F\rangle$, where F is the total spin angular momentum quantum number and m_F is the projection on the spin quantization axis (for systems with more than two spins, additional quantum numbers are necessary).[36] The observable quantity is the total magnetization along the sensitive axis, $\hat{\boldsymbol{s}}$, of the magne-

tometer, represented by the operator

$$O_s = \sum_i \gamma_i \boldsymbol{I}_i \cdot \hat{\boldsymbol{s}}. \quad (2)$$

This operator supports transitions with $\Delta F = 0, \pm 1$. The selection rules for m_F are $\Delta m_F = 0$ if $\hat{\boldsymbol{s}} = \hat{\boldsymbol{z}}$ and $\Delta m_F = \pm 1$ if $\hat{\boldsymbol{s}} = \hat{\boldsymbol{x}}, \hat{\boldsymbol{y}}$.

The Hamiltonian for a pulse with frequency ω and amplitude $\boldsymbol{B}$ is written as

$$H_P(t) = \cos(\omega t) \sum_i \gamma_i \boldsymbol{B} \cdot \boldsymbol{I}_i \quad \equiv \cos(\omega t) P. \quad (3)$$

Evolution of the spin system under the total Hamiltonian $H = H_J + H_P$ is analyzed in an interaction frame where both H_J and H_P are approximately time independent. To this end we consider the interaction frame Hamiltonian when irradiating close to a peak of frequency f and define

$$\tilde{H} = \mathrm{e}^{\mathrm{i}\frac{\omega}{f} H_J t} H \mathrm{e}^{-\mathrm{i}\frac{\omega}{f} H_J t} - \frac{\omega}{f} H_J, \quad (4)$$

where $\tilde{}$ denotes the interaction frame. A more detailed treatment of this process is given in the SI, where we also treat the case of a small static field perturbing H_J, but the result is that the Hamiltonian above can be block diagonalized to a time-independent Hamiltonian acting on a two-level system with each 2x2 block given by

$$\tilde{H} = \begin{pmatrix} \Omega & P_{\alpha\beta} \\ P_{\beta\alpha} & -\Omega \end{pmatrix}, \quad (5)$$

where Ω is the total frequency offset of the transition from ω and the $P_{\alpha\beta}$ are matrix elements of P in the eigenbasis of H_J. If the peak at f involves degenerate energy levels, Eq. 5 holds for each block and the observed signal is the sum of the solutions obtained for each one. Specific conditions for when this is true are given in the SI.

Experimental Methods

We detect ZULF NMR signals using a ^{87}Rb vapor cell magnetometer, operating in the spin-exchange-relaxation-free (SERF) regime [19] and configured for use as an NMR spectrometer,

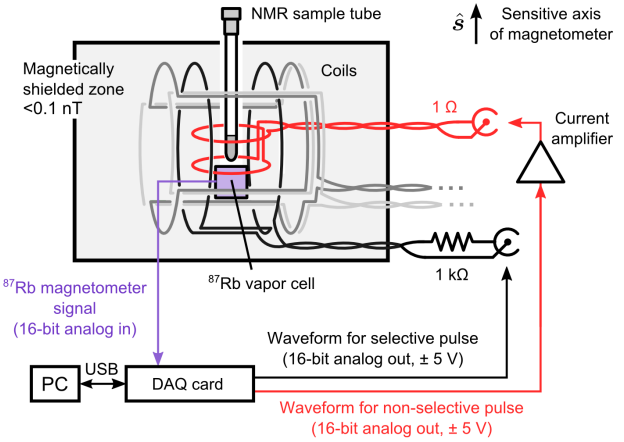

Figure 1: Schematic of the experimental setup. The current amplifier is used to generate strong DC pulses for broadband manipulations. The DAQ in conjunction with the 1 kΩ resistor is used to generate the weak selective AC pulses and bias the static field. The sensitive axis of the magnetometer, denoted $\hat{\boldsymbol{s}}$, lies along the axis of the NMR tube, perpendicular to the plane defined by the pump and probe lasers (not shown).

similar to the setup used in Refs. 13,30,37. Presently the apparatus employs a 5x5x8 mm^3 (inner volume) uncoated glass cell with a small amount of ^{87}Rb metal and 700 Torr N_2 buffer gas (Twinleaf LCC). The cell was kept at 180°C through resistive heating (40 kHz AC) using a twisted wire pair wound around a ceramic pillar (Shapal Hi-M Soft).

In order to generate and control the DC magnetic field pulses we used a National Instruments 6229-DAQ card and a AE Techron LVC2016 linear amplifier in conjunction with a Helmholtz coil (radius = 2.2 cm). The coil was oriented to generate the field along the sensitive axis of the magnetometer. The AC pulses were generated by using three of the ±10 V analog outputs of the DAQ card directly, each output is capable of driving up to 5 mA current and was put in series with a 1 kΩ resistor. The current was fed into three orthogonal 10.5 cm diameter coils placed around the sample, normally used for shimming the field inside the magnetometer. The strength of the magnetic field generated by this process was calibrated by measuring the proton Larmor precession frequency in a sam-

ple of water, the measured frequencies ranged from 0.5 to 4 Hz. The equipment connecting to the various coils is powered from the mains, causing a small oscillating magnetic field inside the shields, observable in the detected spectra at integer multiples of 60 Hz.

Samples ($\sim$150 μL) were placed in standard 5 mm NMR tubes and prepolarized in a 2 T permanent magnet before pneumatic shuttling (over $\sim$0.5 s) to a magnetically shielded region (four layers of μ-metal plus one layer of ferrite, giving a residual field of < 1 μG) for experiment and detection. The DAQ card was also used to control the shuttling and read in the magnetometer response signal, the DAQ was programmed and controlled on a computer using LabVIEW. A schematic of the setup is shown in Fig. 1.

Results and Discussion

We demonstrate selective pulses in zero field using [^{13}C]-methanol ($^{13}CH_3OH$) as an example. The zero-field energy level diagram for the four non-exchanging spins in the molecule, namely the $^{13}CH_3$ group (an AX_3 spin system), is displayed in Fig. 2. There are two observable transitions, one where the total angular momentum quantum number, F, changes from 0 to 1, and another where it goes from 1 to 2. We have taken the spin quantization axis to be parallel to the detector axis, $\hat{\boldsymbol{s}} = \hat{\boldsymbol{z}}$, implying $\Delta m_F = 0$. The two transitions occur at frequencies J_{CH} and $2J_{\mathrm{CH}}$ respectively, where $J_{\mathrm{CH}} = 140.65$ Hz is the one-bond carbon-proton coupling constant. Simultaneous excitation of the two transitions can be achieved using either a DC pulse or non-adiabatic switching to ZULF, affording the spectrum shown in Fig. 2a. The spectra in Figs. 2b/c were recorded after applying selective pulses, at the J_{CH} (0.167 s, B_z =0.94 mG) or $2J_{\mathrm{CH}}$ (0.182 s, B_z =0.94 mG) transition frequencies. Since the bandwidth is much less than the peak separation only the resonant transition is excited. The pulses were applied along the $\hat{\boldsymbol{z}}$ axis in order to excite observable $\Delta m_F = 0$ transitions.

The excitation of the two transitions versus pulse length (Rabi curves) as shown in Figs. 2d/e was used to determine the length of the pulses that gives maximum signal. The J_{CH} signal is expected to be described by $S(t_p) \propto \sin(P_{\alpha\beta}t)$,[38] and thus we expect to see maximum signal for $P_{\alpha\beta}t = \pi/2$. The evaluation of $P_{\alpha\beta}$ may be simplified by noting that the operator can be split into two parts, one proportional to the sum of the spin operators, and one proportional to the difference. The sum term commutes with H_J, and therefore does not induce transitions between states of different F. Thus the relevant matrix elements are $P_{\alpha\beta} = [(\gamma_a B_z - \gamma_b B_z)/2] \langle F', m_F | (I_{a,z} - I_{b,z}) | F, m_F \rangle$, which can be expanded in terms of Clebsch-Gordan coefficients as $P_{\alpha\beta} = [(\gamma_a B_z - \gamma_b B_z)/2] \sum_{m_a,m_b} (m_a - m_b) C^{F',m_F}_{I_a,m_a,I_b,m_b} \times C^{F,m_F}_{I_a,m_a,I_b,m_b}$, where m_F is conserved and a and b refer to the proton and carbon spins. This expression for the matrix element predicts the $1J$ transition to be driven at 1.5 Hz. However, the $2J$ Rabi curve contains two components, using the formula above the frequencies are 1.5 Hz and 1.3 Hz with a relative weighting of 1:2 respectively. The $2J$ Rabi curve being composed of two different frequencies is understood by noting that the line consists of several overlapping transitions, originating in the $m_F = 0$ and the $m_F = \pm 1$ levels and these transitions have different matrix elements. Thus the pulse length that gives maximum signal does not correspond to a single angle. In general the number of frequency components in the Rabi curve is equal to $F_{\max}$ rounded down to the nearest integer. For example both a F=0 to F=1 and a F=1/2 to F=3/2 transition will have one Rabi frequency but a F=2 to F=3 transition will have three.

We now consider the possibilities of selective excitation in the presence of a small perturbing DC field on the order of mG applied at right angles to $\hat{\boldsymbol{s}}$; such small field perturbations have been shown to be useful in ZULF spectroscopy, by splitting lines into multiplets that reveal the quantum numbers involved.[30] The experiments are most conveniently analyzed in a coordinate system where the spin quantization axis is along the direction of the perturbing DC field, so we assign the detection axis to $\hat{\boldsymbol{s}} = \hat{\boldsymbol{x}}$. From

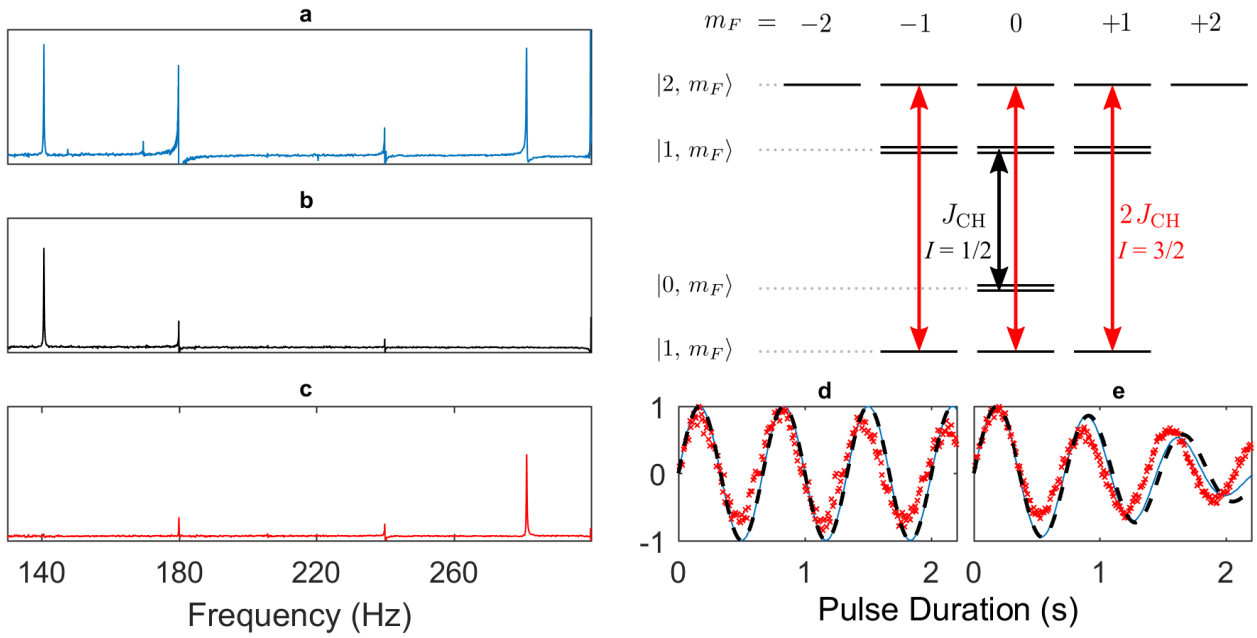

Figure 2: Zero-field NMR of [^{13}C]-methanol. a: When excited by a strong DC pulse the spectrum consists of one peak at $J_{\mathrm{CH}} = 140.65$ Hz and one peak at $2J_{\mathrm{CH}} = 281.3$ Hz. The amplifier used for pulsing generates strong 60 Hz overtones seen in the spectra. b/c: Using weak resonant pulses the transitions can be addressed separately and selectively. The amplifiers used for DC pulsing are turned off, decreasing the 60 Hz noise. d: Signal amplitude versus pulse length, showing the coherent driving between the $|0,0\rangle$ and $|1,0\rangle$ states. Red crosses are experimental data points, the blue line corresponds to $\sin(P_{\alpha\beta}t)$ and the black dashes to a full numerical simulation. e: Driving the $|1,m_F\rangle$ to $|2,m_F\rangle$ transition. The blue line is now a weighted sum of $\sin(P_{\alpha\beta}t)$ for each m_F as described in the text, giving two frequencies. The two observed transitions are shown in the energy level diagram on the right-hand side. I is the quantum number for total proton angular momentum, which is conserved.

this view, observable transitions occur between states where $\Delta m_F = \pm 1$ and the effect of the DC field is to lift degeneracies between states of different m_F, leading to splittings in the spectra. The $\Delta m_F = +1$ and $\Delta m_F = -1$ transitions, in this case correspond to magnetization rotating either clockwise or anticlockwise in the laboratory frame. This is in contrast to the high-field-NMR case where all of the observable transitions correspond to magnetization rotating in the same sense, equal to the direction of Larmor precession around the static field.

The use of two orthogonal pulsing coils to generate a rotating magnetic field allows us to select transitions with $\Delta m_F = +1$ or $\Delta m_F = -1$. Figure 3 shows an example using [^{13}C]-formic acid (H^{13}COOH, an AX spin system, ignoring the exchanging acidic proton). A weak DC field (0.19 mG) is applied at 90° to $\hat{\boldsymbol{s}}$ and the resulting spectrum contains two observable transitions centered about the J-coupling frequency, corresponding to $|0,0\rangle \rightarrow |1,-1\rangle$ and $|0,0\rangle \rightarrow |1,+1\rangle$. A strong DC pulse parallel to $\hat{\boldsymbol{s}}$ simultaneously excites both transitions as shown in Fig. 3a. Figure 3b shows the selective excitation achieved by AC magnetic-field pulses, rotating in the plane defined by $\hat{\boldsymbol{x}}$ and $\hat{\boldsymbol{y}}$: amplitude 0.47 mG, frequency 222.15 Hz (giving a resonance offset of ±0.52 Hz), pulse duration 0.25 s. The coupling matrix element $P_{\alpha\beta}/2\pi$ evaluates to 1.06 Hz using a Clebsch-Gordan expansion similar to the one used above, details in the SI. Although the excitation bandwidth of this pulse covers both transitions they may be addressed selectively based on their sense of rotation, effectively sidestepping the usual limit on

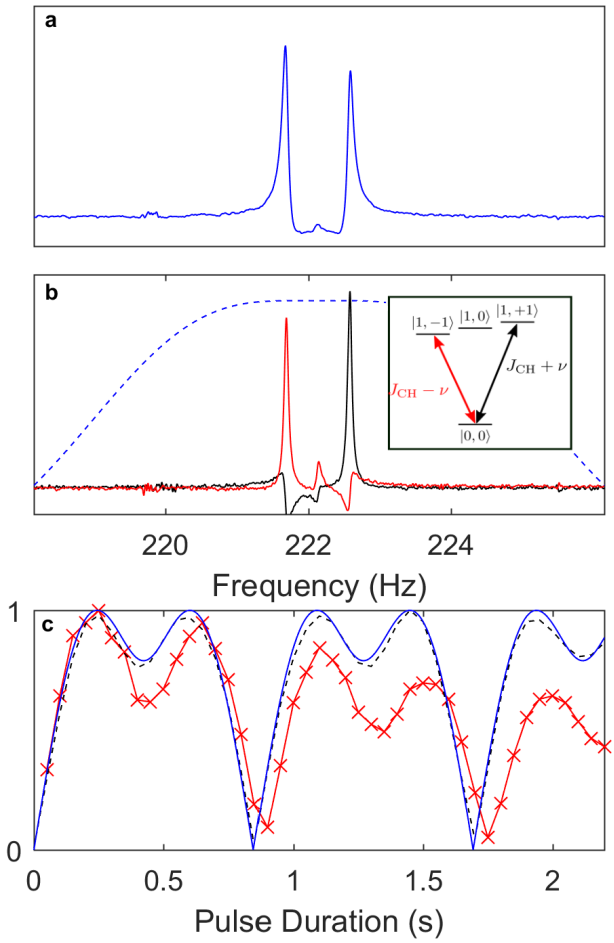

Figure 3: Ultra-low-field NMR (B_0=0.19 mG) of [^{13}C]-formic acid. a: The spectrum after excitation with a DC pulse contains two peaks of equal intensity centered about the J-coupling frequency $J_{CH} = 222.15$ Hz with splitting $2\nu = B_0(\gamma_C + \gamma_H)$. The corresponding transitions are $|0,0\rangle \rightarrow |1,1\rangle$ and $|0,0\rangle \rightarrow |1,-1\rangle$. b: Excitation using a weak near-resonant ($=J_{CH}$) rotating field in opposite senses about the axis of the static field. The dashed blue trace is the expected excitation profile, for the pulse used ($|B| = 0.47$ mG and 0.25 s), defined by the signal magnitude. The inset shows the corresponding energy level diagram. c: Signal magnitude for the $J+\nu$ transition plotted versus pulse length. The red crosses are experimental data, the black dashes to the result of a full numerical simulation, and the blue line corresponds to the predicted signal magnitude when solving for the evolution under Eq. 5, as shown in the SI.

frequency selectivity. The signal magnitude vs. pulse duration for the higher-frequency peak is shown in Fig. 3c to be in quantitative agreement with both the theory and numerical simulation based on the parameters used. The decay of the signal at long pulse lengths may be attributed to relaxation or inhomogeneity of the field.

Selective irradiation may also be used for saturation or population inversion between two or more pairs of spin eigenstates. A "coherence filter" based on this principle is demonstrated in Fig. 4 to edit the zero-field NMR spectrum of [^{15}N,^{13}C$_2$]-acetonitrile (^{13}CH$_3^{13}$C^{15}N). The spectrum nominally contains a large number of observable transitions (>32 different frequencies), but this number can be greatly reduced, and thus assignment of the spectrum made easier, by exciting transitions that share a common energy level. The coherence filter is no more than a difference experiment requiring an even number of signal acquisitions to be performed. Every odd numbered acquisition the full spectrum is excited using a broadband DC pulse parallel to $\hat{\boldsymbol{s}} = \hat{\boldsymbol{z}}$, taking the spin quantization axis parallel to $\hat{\boldsymbol{s}}$ as in our first example (Fig. 2). On even acquisitions, the broadband pulse is preceded by a selective AC pulse, applying the field along the same axis as the DC pulse, which inverts the population difference of a single transition. The difference between the odd and even spectra will contain only peaks corresponding to coherences belonging to the same spin manifold as the inverted transition. Other transitions will remain unchanged by the selective inversion and therefore cancel when the difference spectrum is made. The result of this filtering may be interpreted in the following way: since magnetically equivalent spins will rotate identically about the axis of an applied magnetic field, their total angular momentum cannot change during either the selective inversion pulse or the DC pulse. In the case of [^{15}N,^{13}C$_2$]-acetonitrile a conserved quantum number is the total proton angular momentum, I, which has two possible values ($I = 1/2$ and $I = 3/2$) leading to two isolated spin manifolds. This is also the case for [^{13}C]-methanol, shown in Fig. 2, but for [^{15}N,^{13}C$_2$]-acetonitrile there is additional structure due to presence of more than

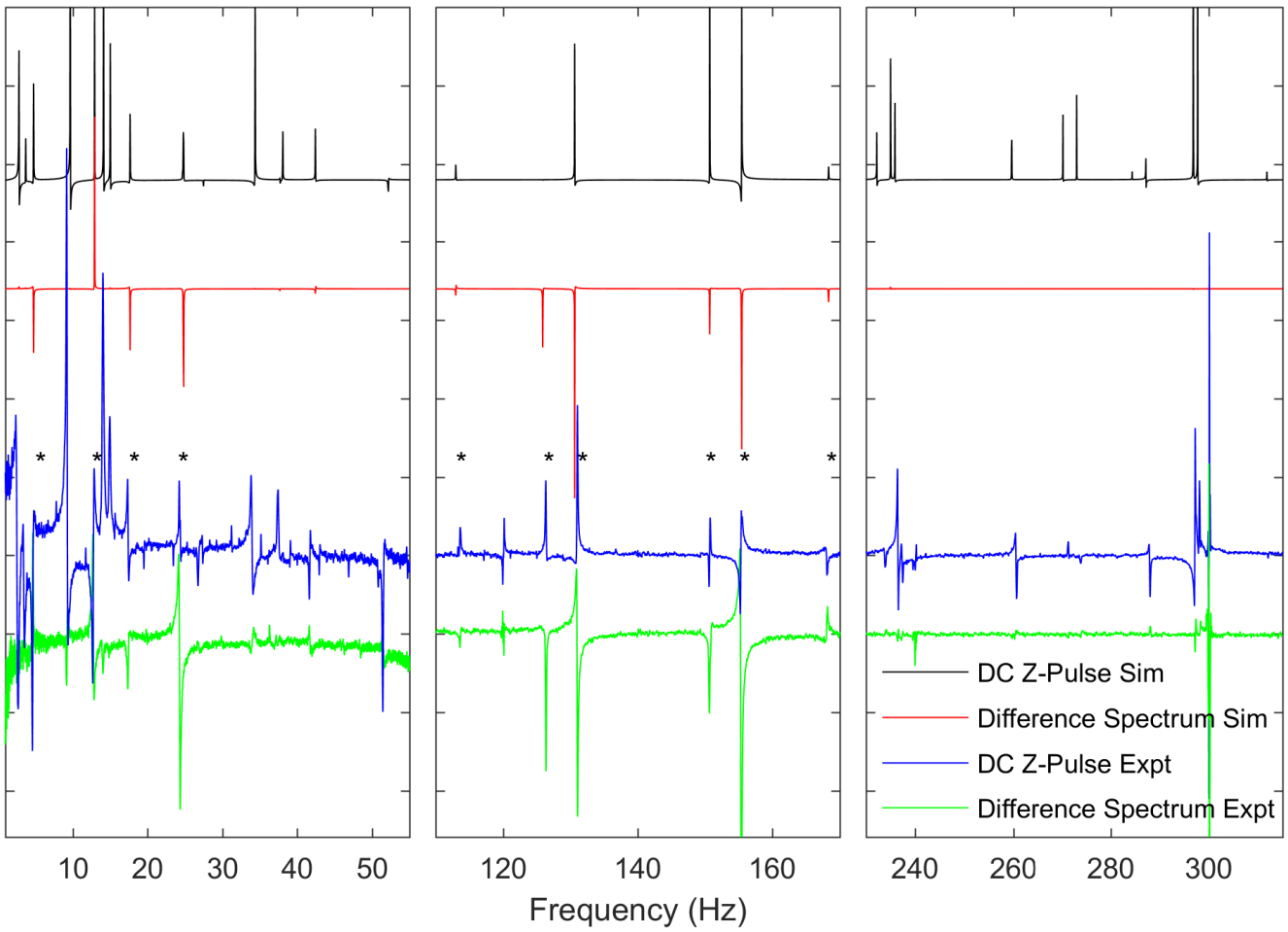

Figure 4: Spectral editing at zero-field. The zero-field spectrum of [^{15}N,$^{13}C_2$]-acetonitrile is split into three different frequency regions for convenience. Bottom blue trace: experimental spectrum recorded after applying a DC pulse in the $\hat{\boldsymbol{s}}$ direction, bottom green trace: Difference spectrum after selective inversion of the 155 Hz line (AC pulse, 0.47 mG, 1.08 s). Stars denote peaks that are still clearly visible in the difference spectrum meaning they belong the $I = 1/2$ manifold. Top Traces: Simulated spectra for the same conditions. The traces are offset for clarity and the peaks at 120 Hz, 240 Hz and 300 Hz are overtones of the 60 Hz line noise.

one J-coupling. The zero-field NMR spectrum is partitioned into three distinct parts. The corresponding signal frequencies are around the one-bond ^{1}H-^{13}C J-coupling frequency at 136 Hz with $I = 1/2$, around $2J = 272$ Hz with $I = 3/2$ and close to 0 Hz arising from the internal splitting of the two manifolds due to the second carbon and the nitrogen. The selective inversion protocol presented here allows us to filter the observed NMR signal and display only peaks belonging to either the $I = 1/2$ or the $I = 3/2$ manifolds.

Figure 4 shows both a simulation of this protocol and the experimental result for the case when the selective inversion pulse is applied at 155 Hz. It is expected that only peaks originating in the $I = 1/2$ manifold to be visible in the difference spectrum. The persistence of the peaks in the region around 136 Hz is consistent with population redistribution within the $I = 1/2$ manifold. There are no observed peaks in the difference spectrum around 272 Hz ($I = 3/2$). The region around zero Hz is the most interesting, four peaks are observed in the difference spectrum so these must belong to the proton spin $I = 1/2$ manifold.

Figure 4 demonstrates another use for selective inversion pulses. Note how in the simula-

tion the peak at ≈126Hz is not visible in the control spectrum, but is clearly apparent in the difference spectrum. This indicates that before the DC pulse there is no population difference between the two states involved. The selective inversion pulse swaps the initial population of one of the two states with a third state so that the population difference becomes nonzero. This is analogous to the technique of interchanging spin populations for signal enhancement in NMR studies of quadrupolar nuclei.[39] In the experimental data, the peak at ≈ 126 Hz also becomes significantly enhanced. However, the peak is also visible in the control spectrum, which we attribute to the sensitive axis of the magnetometer being slightly off-axis from $\hat{\boldsymbol{z}}$.[16]

Conclusions

In conclusion we have demonstrated selective excitation and editing of zero-field J-spectra using weak AC fields. Simple analytical theory based on a two-level system reproduces the results from full numerical simulations and experiments. As a chemically relevant application we have shown a method that discriminates between signals belonging to manifolds of different total proton angular momentum in the zero-field spectrum of [^{15}N,$^{13}C_2$]-acetonitrile. Further we have shown how the sense of rotation of pulsed fields may select between positive and negative changes in angular-momentum projection. These techniques should facilitate zero-field NMR spectroscopy of larger, more demanding spin systems or mixtures, and open a way to adapting a suite of established high-field experiments to zero-field.

Acknowledgement The authors thank J. W. Blanchard for helpful discussions. This work was supported by the National Science Foundation under award CHE-1308381 and in part by the Director, Office of Science, Office of Basic Energy Sciences, Materials Sciences and Engineering Division, of the U.S. Department of Energy under Contract No. DE-AC02-05CH11231 (JPK). This work was supported by the European Commission under the Marie Curie International Outgoing Fellowship Programme (author MCDT, project FP7-625054 ODMR-CHEM). Contents of the work do not reflect the views of the university or the European Commission.

Supporting Information Available: Derivation of equations for the signal magnitude as a function of resonance offset and pulse length. More detailed evaluation of matrix elements. Details regarding the simulations. This material is available free of charge via the Internet at `http://pubs.acs.org/`.

References

(1) Jameson, C. J. *Annual Review of Physical Chemistry* **1996**, *47*, 135–169.

(2) Kumar, A.; Wagner, G.; Ernst, R. R.; Wüthrich, K. *Journal of the American Chemical Society* **1981**, *103*, 3654–3658.

(3) Yao, L.; Vögeli, B.; Ying, J.; Bax, A. *Journal of the American Chemical Society* **2008**, *130*, 16518–16520.

(4) Berger, S.; Braun, S. *200 and more NMR experiments: a practical course.*, 3rd ed.; Weinheim: Wiley-Vch: Chicago, 2004.

(5) Caravatti, P.; Bodenhausen, G.; Ernst, R. *Journal of Magnetic Resonance* **1983**, *55*, 88–103.

(6) Freeman, R. *Chem. Rev.* **1991**, *91*, 1397–1412.

(7) McCoy, M. A.; Mueller, L. *J. Am. Chem. Soc.* **1992**, *114*, 2108–2112.

(8) Bax, A. *Journal of Magnetic Resonance* **1984**, *57*, 314–318.

(9) Bax, A.; Ferretti, J. A.; Nashed, N.; Jerina, D. M. *The Journal of Organic Chemistry* **1985**, *50*, 3029–3034.

(10) Kessler, H.; Oschkinat, H.; Griesinger, C.; Bermel, W. *Journal of Magnetic Resonance* **1986**, *70*, 106–133.

(11) Thayer, A., M.; Luzar, M.; Pines, A. *Journal of Magnetic Resonance* **1987**, *72*, 567–573.

(12) Zax, D. B.; Bielecki, A.; Zilm, K. W.; Pines, A. *Chemical Physics Letters* **1984**, *106*, 550–553.

(13) Ledbetter, M. P.; Crawford, C. W.; Pines, A.; Wemmer, D. E.; Knappe, S.; Kitching, J.; Budker, D. *Journal of Magnetic Resonance* **2009**, *199*, 25–29.

(14) Blanchard, J. W.; Budker, D. *eMagRes* **2016**, *Accepted Manuscript*.

(15) Blanchard, J. W.; Ledbetter, M. P.; Theis, T.; Pines, A. *Journal of the American Chemical Society* **2013**, *135*, 3607–3612.

(16) Blanchard, J. W.; Sjolander, T. F.; King, J. P.; Ledbetter, M. P.; Levine, E. H.; Bajaj, V. S.; Budker, D.; Pines, A. *Physical Review B - Condensed Matter and Materials Physics* **2015**, *92*, 1–6.

(17) Budker, D.; Romalis, M. *Nature Physics* **2007**, *3*, 227–234.

(18) Schwindt, P. D. D.; Knappe, S.; Shah, V.; Hollberg, L.; Kitching, J.; Liew, L. A.; Moreland, J. *Applied Physics Letters* **2004**, *85*, 6409–6411.

(19) Seltzer, S. J. Developments in Alkali-Metal Atomic Magnetometry. Ph.D. thesis, Princeton, 2008.

(20) McDermott, R.; Trabesinger, A. H.; Muck, M.; Hahn, E. L.; Pines, A.; Clarke, J. *Science* **2002**, *295*, 2247–2249.

(21) Matlachov, A. N.; Volegov, P. L.; Espy, M. A.; George, J. S.; Kraus, R. H. *Journal of Magnetic Resonance* **2004**, *170*, 1–7.

(22) Bernarding, J.; Buntkowsky, G.; Macholl, S.; Hartwig, S.; Burghoff, M.; Trahms, L. *Journal of the American Chemical Society* **2006**, *128*, 714–715.

(23) Hartwig, S.; Voigt, J.; Scheer, H. J.; Albrecht, H. H.; Burghoff, M.; Trahms, L. *Journal of Chemical Physics* **2011**, *135*, 1–5.

(24) Savukov, I. M.; Romalis, M. V. *Physical Review Letters* **2005**, *94*, 1–4.

(25) Ledbetter, M. P.; Savukov, I. M.; Budker, D.; Shah, V.; Knappe, S.; Kitching, J.; Michalak, D. J.; Xu, S.; Pines, A. *Proceedings of the National Academy of Sciences of the United States of America* **2008**, *105*, 2286–2290.

(26) Liu, G.; Li, X.; Sun, X.; Feng, J.; Ye, C.; Zhou, X. *Journal of Magnetic Resonance* **2013**, *237*, 158–163.

(27) Bevilacqua, G.; Biancalana, V.; Baranga, A. B.-A.; Dancheva, Y.; Rossi, C. *Journal of Magnetic Resonance* **2015**, *263*, 65–70.

(28) Theis, T.; Blanchard, J. W.; Butler, M. C.; Ledbetter, M. P.; Budker, D.; Pines, A. *Chemical Physics Letters* **2013**, *580*, 160–165.

(29) Shim, J. H.; Lee, S.-J.; Hwang, S.-m.; Yu, K.-K.; Kim, K. *Journal of Magnetic Resonance* **2014**, *246*, 4–8.

(30) Ledbetter, M. P.; Theis, T.; Blanchard, J. W.; Ring, H.; Ganssle, P.; Appelt, S.; Blümich, B.; Pines, A.; Budker, D. *Physical Review Letters* **2011**, *107*, 1–5.

(31) Appelt, S.; Häsing, F. W.; Sieling, U.; Gordji-Nejad, A.; Glöggler, S.; Blümich, B. *Physical Review A - Atomic, Molecular, and Optical Physics* **2010**, *81*, 1–11.

(32) Freeman, R.; Anderson, W. A. *The Journal of Chemical Physics* **1962**, *37*, 2053–2073.

(33) Freeman, R.; Gestblom, B. *The Journal of Chemical Physics* **1967**, *47*, 2744.

(34) Shim, J. H.; Lee, S. J.; Yu, K. K.; Hwang, S. M.; Kim, K. *Journal of Magnetic Resonance* **2014**, *239*, 87–90.

(35) Thayer, A., M.; Pines, A. *Journal of Magnetic Resonance* **1986**, *70*, 518–522.

(36) Butler, M. C.; Ledbetter, M. P.; Theis, T.; Blanchard, J. W.; Budker, D.; Pines, A. *Journal of Chemical Physics* **2013**, *138*.

(37) Tayler, M. C. D.; Sjolander, T. F.; Pines, A. *Journal of Magnetic Resonance* **2016**,

(38) Pileio, G.; Carravetta, M.; Levitt, M. H. *Physical Review Letters* **2009**, *103*, 1–4.

(39) Kentgens, A.; Verhagen, R. *Chemical Physics Letters* **1999**, *300*, 435–443.

Graphical TOC Entry